J Solid State Electrochem (2010) 14:93–99
DOI 10.1007/s10008-009-0793-6

ORIGINAL PAPER

Kinetic studies of underpotential deposition of antimony on Se-modified Au electrode

Xuezhao Shi · Xin Zhang · Chuanli Ma · Chunming Wang

Received: 8 November 2008 / Revised: 18 January 2009 / Accepted: 23 January 2009 / Published online: 8 February 2009

Abstract Atomic layers of antimony can be electrodeposited onto the Se monolayer covered Au electrode in the underpotential region. In this paper, the formation and dissolution kinetics of antimony monolayer on the Se monolayer covered Au electrode are investigated using cyclic voltammetry (CV) and chronoamperometry (CA) techniques. Scanning-rate-dependent CV experiments reveal that the peak current of underpotential deposition (UPD) wave of antimony is not a linear function of the scanning rate, υ, but scales as $\upsilon^{2/3}$. Similar behavior is observed when the Antimony monolayer is stripped from the modified substrate. These results indicate the character of monolayer formation and dissolution by a two-dimensional nucleation and growth mechanism. Additionally, current density−time transient obtained through CA experiments also reveal that both the deposition and stripping of the antimony monolayer involve an instantaneous nucleation and two-dimensional growth process.

Keywords UPD · CV · CA · Antimony

Introduction

Antimony selenide, a member of V–VI semiconductor with a layer-structured semiconductor of orthorhombic crystal structure, has attracted much attention in recent years due to its good photoconductivity and thermal electronic properties [1, 2], which allow possible applications for micro- and optoelectronic and biomedical fields, such as in situ powering or minicooling integrated circuit (IC) chips, optoelectronic sensors, micro-electro-mechanical system (MEMS) devices, and biochips [3]. Various methods such as chemical baths in aqueous and non-aqueous solutions, spray, vacuum evaporation, electrodeposition techniques, etc. have been used for preparation of Sb_2Se_3 film [2, 4–7]. Of all this preparation techniques, electrodeposition is a simple, convenient, quick and economical method for the preparation of thin films but leads to polycrystalline deposits. Recently, Stickney and coworkers have developed an electrochemical analog of conventional atomic layer epitaxy which has been used to produce a wide variety of well-ordered semiconductor deposits [8–10]. Electrochemical atomic layer epitaxy (EC-ALE) takes advantage of UPD phenomenon [10], where the electrodepostion of a metal on a foreign metal at potentials less negative than the equilibrium potential of the deposition reaction. Such a process is energetically unfavorable and it can occur only because of a strong interaction between the two elements, with their interaction energy changing the overall energies to favorable. If the process is oxidative, the potential is less positive. The resulting deposit is generally limited to an atomic layer. This method has been used to grow many binary compound thin film deposits in a layer-by-layer pattern, including CdS [11, 12], Bi_2Te_3 [13, 14], SnSe [15], and CdTe [16, 17].

Our interests are in the kinetics of initial layer of Sb_2Se_3 super-thin film formed by the EC-ALE technique. Understanding the formation kinetics of the first monolayer is crucial to achieving an atomic-level of any interface. However, no study has been done on the growth of Sb_2Se_3 thin films. Chronoamperometric and voltammetric techniques are useful tools for understanding the kinetics of thin film formation involved in UPD.

X. Shi · X. Zhang · C. Ma · C. Wang (✉)
Department of Chemistry, Lanzhou University,
Lanzhou 730000, People's Republic of China
e-mail: wangcm@lzu.edu.cn

In this paper, cyclic voltammetric and chronoamperometric techniques were used to investigate the deposition and stripping kinetics of antimony on Se-modified gold electrode. Analysis of the CV data suggests that the deposition and stripping of antimony on Se-modified gold surface in the underpotential region proceed by a two-dimensional nucleation and growth mechanism in terms of two-dimensional phase transition model developed by Maestre et al. [18]. Besides the CV data, current–time transients were analyzed using two-dimensional nucleation and growth model which was developed by Fleischmann [19, 20]. Potential step experiments indicates that the kinetics of monolayer of antimony on Se-modified gold surface proceeds an instantaneous two-dimensional nucleation and growth mechanism and its stripping also proceeds an instantaneous two-dimensional mechanism.

Experimental

The electrochemical cell used for these studies consists of a conventional three-electrode system and a CHI 660A electrochemical workstation (CH Instrument, USA). The auxiliary electrode was a platinum foil, and saturated calomel electrode (SCE) served as the reference electrode. The substrate was a polycrystalline gold disk electrode. The gold substrates were polished with successively finer grades of alumina powder down to 0.05 μm and then cleaned ultrasonically in twice-distilled water for 5 min. Before the electrochemical experiments were conducted, an electrochemical polishing process was carried out using CV technique in freshly prepared 0.10 M $HClO_4$ between 1.0 and −0.5 V to assure surface cleanliness.

Antimony deposition solutions consisted of 1 mM trihydrate antimony potassium tartrate with 1 M hydrochloric acid as supporting electrolyte. Selenium deposition solutions consisted of 1 mM selenium dioxide with 0.10 M perchloric acid solution used as supporting electrolyte. The blank solution was 0.10 M perchloric acid and 1 M hydrochloric acid. Water used for solutions was purified by the Milli-Q system (Millipore Inc., nominal resistivity 18.2 MΩ cm), and the chemicals were reagent-grade or better. Prior to each experiment, all the solutions were carefully deaerated by blowing purified N_2.

Results and discussion

Formation of Se atomic layers on Au

The cyclic voltammograms of Au electrode immersed in 1 mM SeO_2 in 0.10 M $HClO_4$ supporting electrolyte is shown in Fig. 1. In order to confirm the UPD peak of Se on

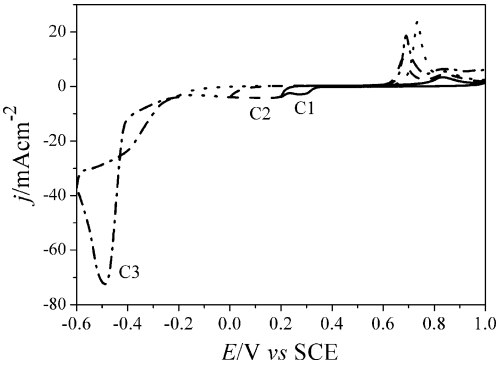

Fig. 1 Cyclic voltammograms of Au electrode in 1 mM SeO_2. Supporting electrolyte, 0.10 M $HClO_4$; scanning rate, 20 mV/s

Au electrode, the potential scans negatively from an initial potential of 1.00 V to different negative potentials 0.20, 0.00, −0.20, and −0.60 V. Three major reductive peaks (denoted C1–C3) are observed. Peak C1 is attributed to the surface-limited wave which is qualitatively similar to the UPD peaks observed for the reduction of metals on high work function substrates [21, 22] and the charge density for this peak was calculated as 443 μC cm^{-2} ,the corresponding coverage for it was 0.46 ML, as expected for UPD of Se; a ML in this case refers to an elemental atom layer relative to the number of Au substrate surface atoms, a ratio of 1.0 refers to a full monolayer (ML); the broad-feature-labeled C2 corresponds to the bulk deposition of Se which also include some underpotential deposited Se because the deposition of Se on gold substrate do not process typical underpotential deposition process [21, 23]. Peak C3, occurring at a potential of about −0.50 V, corresponds to the reduction of adsorbed Se(0) to Se(−II) which then undergoes a comproportionation reaction with Se(IV) in solution, leading to the chemical formation of Se(0) according to the following reaction [24]:

$$H_2SeO_3 + 2H_2Se \rightleftarrows 3Se + 3H_2O \quad (1)$$

At more negative potentials, the direct reduction of Se (IV) to Se (−II) also occurred, with transference of six electrons, in accordance with the following equation [25]:

$$H_2SeO_3 + 6H^+ + 6e^- \rightleftarrows H_2Se\uparrow + 3H_2O \quad (2)$$

It has been reported that the deposition of Se does not show classical UPD process [21, 23], while requires an overpotential, but bulk deposition of Se is so slow that a surface-limited feature is still visible. Therefore, the following method was employed to obtain a monolayer of Se on the Au substrate. Namely, an overpotential was selected to deposit Se, which resulted in a small amount of bulk deposited Se along with the surface-limited reaction, and then an extra step was introduced to remove the bulk deposition Se by reducing the bulk deposition Se to a gaseous species, hydrogen selenide H_2Se, which bubbled

out from the solution, leaving the only underpotentially deposited Se on gold surface:

$$Se_{upd} + Se_{bulk} + 2e^- + 2H^+ \rightleftarrows Se_{upd} + H_2Se \uparrow \quad (3)$$

Consequently, the suggested procedure to obtain an UPD layer of selenium consists of depositing an excess of selenium at −0.25 V for 20 s and then applying a potential of −0.55 V for 3 s in the blank solution, which was negative enough to reduce bulk deposited selenium, but not the underpotentially deposited selenium. After this deposition process, charge density for deposition of Se on gold substrate was 764 μC cm^{-2}.

Figure 2 show stripping voltammograms of selenium in 0.1 M $HClO_4$ blank solution from the gold electrode. As was shown from curve 1 in Fig. 2, selenium stripping exhibited two peaks B2 (0.74 V) and B1 (0.81 V). B1 probably corresponds to dissolution of the adlayer bonded to the gold substrate, while B2 corresponds to the bulk layers deposited on the selenium adlayer [15]. As E_d was shifted from −0.15 to −0.25 V (curve1 to curve3), the height of the stripping peak changed progressively to larger values, which showed that the amount of reductive selenium increased. When the stripping process was brought in after deposited in −0.25 V for 20 s, maintained at −0.55 V for 3 s, the corresponding stripping voltammogram was also shown in Fig. 2 (curve 4). From curve 4 in Fig. 2, only one peak (0.83 V) corresponding to the stripping of selenium adlayer was observed. That is to say, after this deposition process only underpotentially deposited selenium remained on the electrode surface.

Cyclic voltammetry of antimony on Se-modified Au

Figure 3a shows the CV curve of bare Au electrode in 1 mM antimony solution, with potential successively scanning from 0.50 V to different cathodic limits (−0.1, −0.2, −0.3, and −0.5 V, respectively). In Fig. 3a, we could observe that peak A2 became higher as the potential scanned negatively, while peak A1 remained a constant value. Therefore, peaks C1 and A1, occurring at 0.03 and 0.13 V, respectively, are attributed to the UPD and UPD stripping of antimony on Au. Fig. 3b shows the deposition and stripping voltammetry of antimony on Se-modified Au substrate (solid line). The CV curve of antimony deposition and stripping on the bare Au substrate (dashed line) is also shown in Fig. 3b for comparison. The electrochemistry of antimony on Se-modified Au surface is noticeably different from the voltammetry at bare Au substrate. Both the UPD peak, labeled as C1 in Fig. 3b on the solid line occurring at about −0.13 V, and the bulk deposition peak, labeled as C2 occurring at about −0.32 V, shift to less positive potentials compared with that on bare Au electrode. Anodic stripping peaks, which consist of a shaper peak at −0.08 V and a broad one at 0.21 V, appears on the positive scanning. Peak A1, corresponding to the UPD stripping peak, is broad and shifts to more positive potentials, while for peak A2, only a little positive shift is observed compared with that on bare Au. Two comparative factors should be responsible for the shift of peaks in Fig. 3. One was the slow electron-transfer kinetics, which was caused by the heteroepitaxial structure and work function difference between the predeposited Se monolayer and Au electrode. It will block the current and

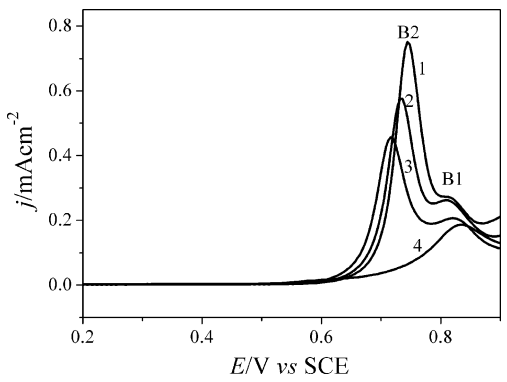

Fig. 2 The differential pulse anodic stripping voltammograms (DPASV) curves of Se (IV) in 0.1 M $HClO_4$ solution deposited at different potentials for 20 s: (*1*) E_d = −0.25 V, (*2*) E_d = −0.20 V, (*3*) E_d = −0.15 V, (*4*) E_d = −0.25 V, then E_s = −0.55 V, t = 3 s in blank solution

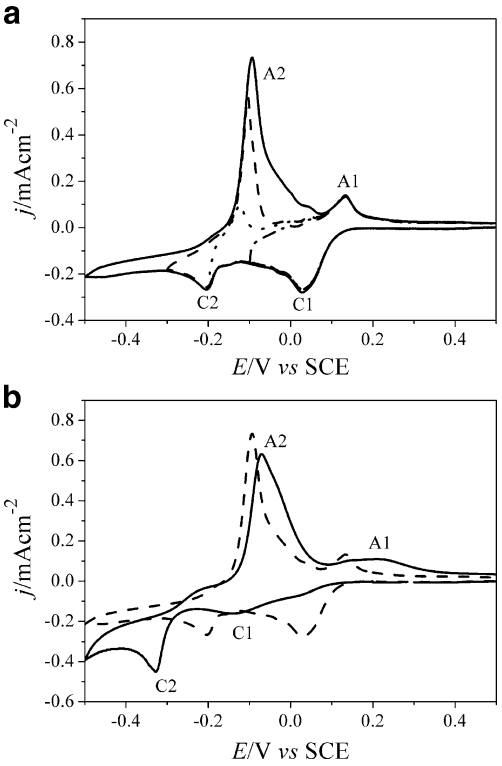

Fig. 3 **a** Cyclic voltammograms of Au in 1 mM antimony. Scan rate: 20 mV/s. **b** Cyclic voltammetry of Se-modified Au substrate (*solid line*) and bare Au electrode (*dashed line*) in antimony solution

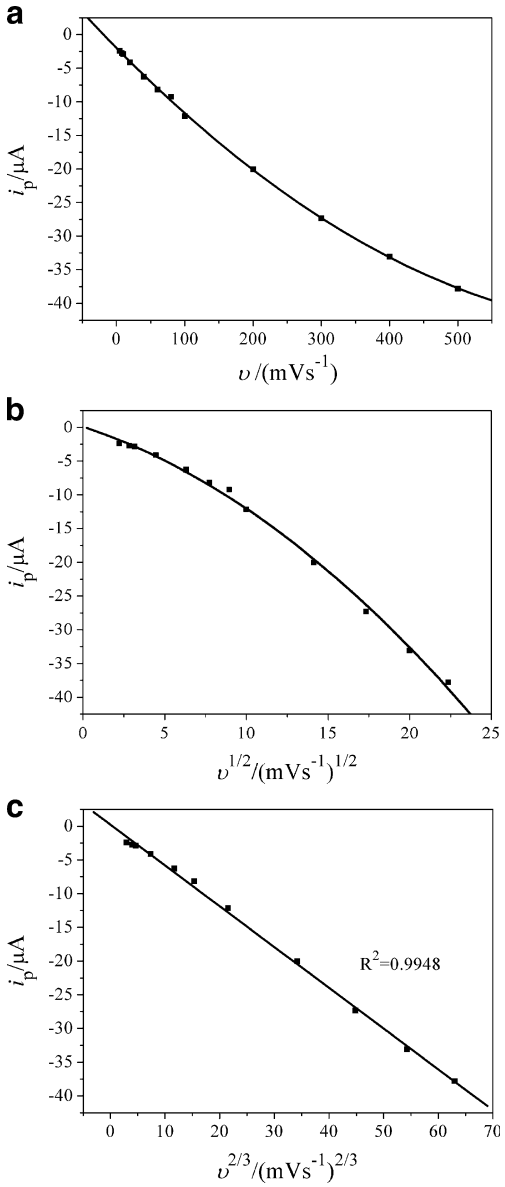

Fig. 4 Scanning-rate dependence of the antimony deposition wave on Se-modified Au electrode: **a** dependence of the peak current in C1 on the scanning rate, υ. **b** dependence of the peak current in C1 on $\upsilon^{1/2}$. **c** Dependence of the peak current in C1 on $\upsilon^{2/3}$

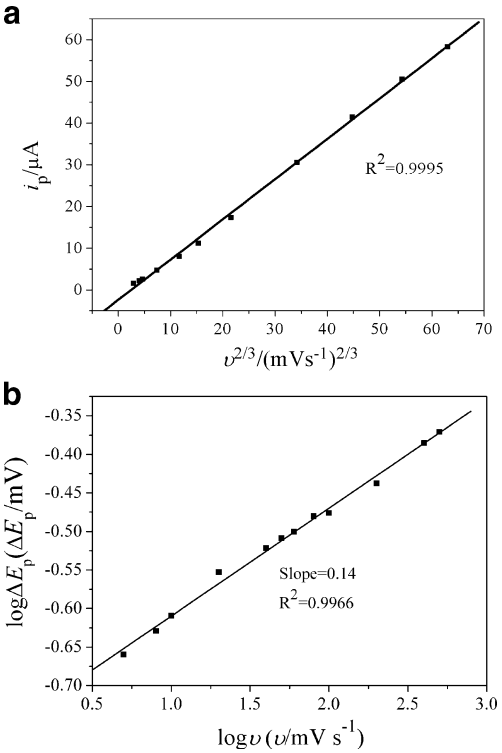

Fig. 5 **a** Scanning rate dependence of the antimony stripping wave. Dependence of the peak current A1 on $\upsilon^{2/3}$. **b** Plot of log ΔE_p *vs* log υ for the A1/C1 couples

partake a part of the potential, making the reductive peak shift to more negative potential and the stripping peak shift to more positive potential. The other was the stronger interaction between antimony and the predeposited Se adlayer than that between antimony and the Au substrate which will lead to the formation of Sb_2Se_3 compounds. It will make antimony deposition occur at a more positive potential than that on the uncovered Au electrode. In Fig. 3, deposition of antimony on the Se-modified electrode shifted to more negative potentials and the striping peak shifted to more positive potentials, indicating that slow electron-transfer-kinetic effect predominated over the deposition and stripping process. On the Se-modified Au substrate, except the bulk deposition peak C2, the magnitude of the other three peaks C1, A1, and A2 were smaller than that on the bare Au substrate. For peak C2, the increase of current strength may be attributed to the formation of Sb_2Se_3 compound through the following reaction:

$$2Sb(III) + 3Se + 6e^- \rightleftarrows Sb_2Se_3 \quad (4)$$

With regard to peaks C1 and A1, the decrease of the current strength may be attributed to the slow electron-transfer kinetics caused by the predeposited Se monolayer, while for peak A2, besides this slow electron-transfer kinetics, the decrease may also caused by reaction (4). The underpotential shift, ΔE_p, the difference between the UPD potential and bulk deposition potential ($E_{Sb(III)/Sb}$), on the Se-modified Au surface was smaller than that on bare Au substrate. This result indicated that the deposition of antimony at −0.13 V on Se-covered Au surface required more energy than the deposition on bare Au substrate.

In the cyclic voltammograms, the peak current for adsorption wave, $(i_p)_{ads}$, increases linearly with the scanning rate, υ, while that for the diffusion wave, $(i_p)_{diff}$, increases linearly with the square root of scanning rate, $\upsilon^{1/2}$. Figure 4 shows the scanning-rate dependence of Antimony deposition current peaks on Se-modified Au substrate. The peak currents for C1 were non-linear when plotted versus the square root of the scanning rate, ruling out the

possibility of diffusion-limited mass transport of antimony species to the substrate surface (Fig. 4b). Positive deviations from linear scanning-rate dependence at high scanning rates may be attributed to slow electron-transfer kinetics. If the peak currents were plotted as a function of 2/3 the power of the scanning rates, the plot for C1 was linear over the entire range of scanning rates we studied (Fig. 4c). A $\upsilon^{2/3}$ scanning-rate dependence is characteristic of a two-dimensional phase transition or a two-dimensional nucleation and growth mechanism [18]. A similar scanning-rate behavior was observed for anodic stripping peak A1, and a plot of the dependence of the peak current on 2/3 the power of the scanning rates, $\upsilon^{2/3}$ was shown in Fig. 5a. According to voltammetric data, we concluded that deposition of antimony on Se-modified Au substrate proceeded by a two-dimensional nucleation and growth mechanism and the stripping also proceeded a two-dimensional process. The model mentioned by Maestre et al. [18] suggests an additional criterion for 2-D nucleation and growth, namely a log–log plot of the peak separation, ΔE_p, between peak potentials and the scanning rate should have a slope of 2/5. A plot of $\log\Delta E_p$ against $\log\nu$ was shown in Fig. 5b. We calculated a value of 0.14 for the slope obtained from the A1/C1 waves, which was smaller than the predictions values in this model. This might be attributed to the irreversibility of deposition/stripping of antimony under high scanning rates.

Chronoamperometry of antimony on Se-modified Au

For better understanding of the growth mechanism of antimony on Se-covered Au substrate in more detail, potential step experiments were performed for both the deposition and stripping of antimony on the Se-modified Au surface. In order to eliminate the double-layer charging currents from the transients, the background transient obtained in the absence of Sb^{3+} was taken and subtracted electronically from those obtained in the presence of Sb^{3+}. Typical current density–time transients for deposition and stripping of antimony on the Se-modified Au substrate are presented in Fig. 6a. As can be seen, the shapes of the current density–time transients for both the deposition peak and the stripping peak shows the character of a two-dimensional nucleation and growth model, which was also consistent with the CV data. The corresponding charge density for deposition of antimony was calculated as 366 μC cm^{-2}. Moreover, it was also observed from the potential step measurements that both of the deposition and the stripping proceeded rapidly, completing in only several tens of milliseconds.

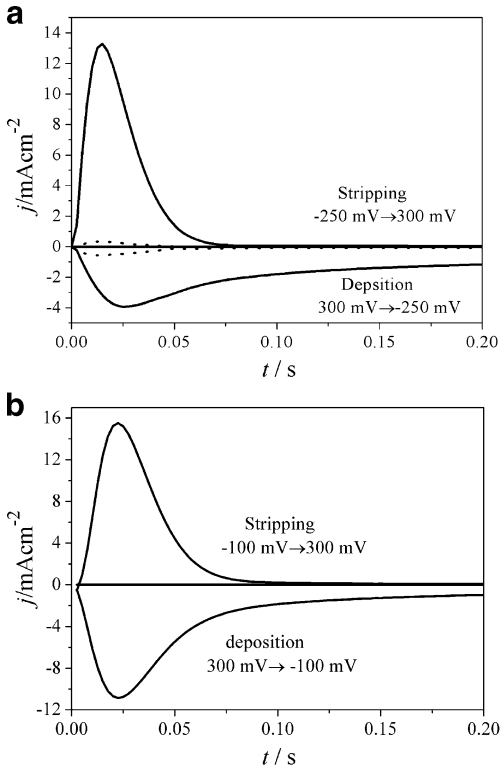

Fig. 6 **a** Current density–time transients for antimony deposition and stripping on Se-modified Au electrode and background transients (*dotted line*); **b** current density–time transients for antimony deposition and stripping on bare Au electrode

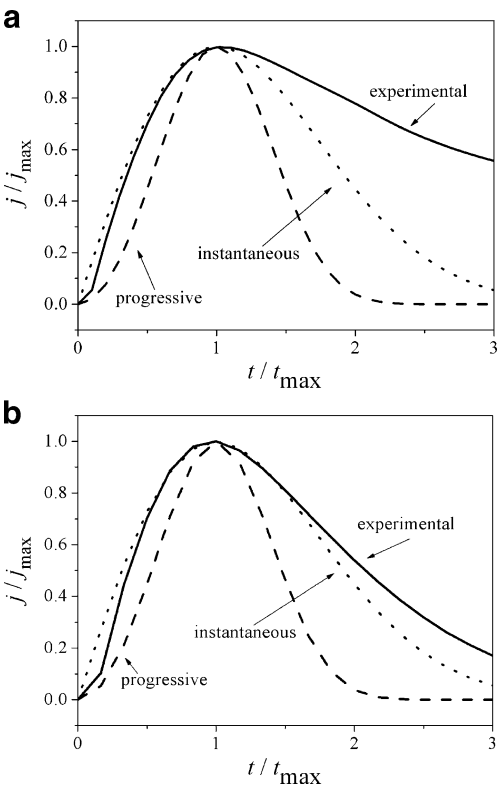

Fig. 7 Representative reduced variable plot showing fit to instantaneous and progressive nucleation models. **a** Deposition process; **b** stripping process

Figure 6b shows typical current density–time transients for deposition and stripping of antimony on the bare Au substrate. Due to deposition and stripping of antimony on Se-modified Au and bare Au substrate occurring at different potentials, different step potentials were selected for that on bare Au substrate and Se-modified Au substrate. From Fig. 6b, we could see that the peak current densities of the transients on Se-modified Au electrode were lower than those on the bare Au electrode under the same overpotentials, which should also be attributed to the slow electron-transfer kinetics.

Nowadays, the kinetics of monolayer formation by 2-D nucleation and growth has been well understood [26–29]. The experimental current–time transients were fit to two limiting cases: instantaneous nucleation, when the nucleation rate is large and the maximum number of nuclei is formed as soon as the potential is stepped, and progressive nucleation, when the nucleation rate is small and remains constant on the time scale of the experiment. Current density–time transients are described by the following equations:

$$j_{\text{inst}} = at\exp\left(-bt^2\right) \tag{5}$$

for the instantaneous case and

$$j_{\text{prog}} = ct^2\exp\left(-dt^3\right) \tag{6}$$

for the progressive case. In the above two equations, the pre-exponential term gives the current density into the step edges of the independently growing nuclei (i.e., the asymptotic behavior at short times). The exponential term corrects for the decreased step edge length due to the overlap of adjacent nuclei at longer times. In a potential step experiment a, b, c, and d are constants; explicit formulas can be found in the review by Budevski [30]. Experimental current density–time transients were fit using the so-called reduced variable plots following the procedure of Bewick, Fleischmann, and Thirsk [19, 20]. Therefore, we could know that two-dimensional nucleation and growth can also be described as either instantaneous or progressive. Comparison of the reduced variable plot of the measured quantities ($j/j_{\max}$ vs $t/t_{\max}$) with those calculated by Eqs. (5) and (6) allows us to distinguish between these two types of nucleation behavior. Figure 7a shows the reduced variable plots for the deposition transients shown in Fig. 6a. Calculated transients for instantaneous and progressive nucleation are also shown for direct comparison with the experimental data. The reduced variable plot indicated that before, the maximum deposition mechanism was instantaneous, which indicated that the maximum number of nuclei formed at the beginning of the potential step. While after the maximum, positive deviation of experimental curve from calculated values should be caused by adsorption of counter ion.

A similar analysis was carried out for stripping of antimony on Se-modified Au electrode. Figure 7b shows the reduced variable plots for the stripping transients shown in Fig. 6a and the calculated transients for instantaneous and progressive dissolution process, which were very similar to that obtained for the deposition process. The reduced variable plot showed that the nucleation and growth kinetics also fits reasonably well to the instantaneous model, indicating that the dissolution sites were activated at the beginning of potential step and keeping constant during the stripping process.

Conclusion

We have investigated the electrochemistry behavior of Antimony on Se-modified Au electrode using CV and CA techniques in order to understand the kinetics of the first Sb_2Se_3 layer growth when Se was deposited firstly. The charge density for Se and antimony were 764 μC cm^{-2} and 366 μC cm^{-2}, respectively, indicating Sb/Se atomic ratio of 0.64 in agreement with the stoichiometric ratio of the Sb_2Se_3 compound, 0.67. We find that the formation and dissolution of the antimony monolayer on Se-modified Au electrode proceeds by a two-dimensional nucleation and growth mechanism in the underpotential region. Additionally, current density–time transients obtained from CA experiments indicate that the formation of monolayer antimony on Se-modified gold surface proceeds an instantaneous two-dimensional nucleation and growth mechanism in the short-time region, while in the long-time region experimental curve deviates from the calculated values which should be caused by adsorption of counter ion. For stripping process, it proceeds an instantaneous two-dimensional mechanism in whole time region.

Acknowledgment Supported by the National Natural Science Foundation of China (Grant No. 20577017 B0701).

References

1. Fan KX, Zeng G, LaBounty C, Bowers JE, Croke E, Ahn CC, Huxtable S, Shakouri A (2001) Appl Phys Lett 78:1580. doi:10.1063/1.1356455
2. Rajapure Y, Lokhande CD, Bhosele CH (1997) Thin Solid Films 311:114. doi:10.1016/S0040-6090(97)00415-X
3. Yang JY, Zhu W, Gao XH, Bao SQ, Fan XA, Duan XK, Hou J (2006) J Phys Chem B 110:4599. doi:10.1021/jp0565498
4. Mane RS, Sankapal BR, Lokhande CD (1999) Mater Chem Phys 60:196. doi:10.1016/S0254-0584(99)00085-1
5. Fernaández AM, Merino MG (2000) Thin Solid Films 366:202. doi:10.1016/S0040-6090(00)00716-1
6. Rajpure KY, Bhosale CH (2000) Mater Chem Phys 62:169. doi:10.1016/S0254-0584(99)00173-X

7. Torane AP, Bhosale CH (2002) J Phys Chem Solids 63:1849. doi:10.1016/S0022-3697(02)00167-1
8. Gregory BW, Stickney JL (1991) J Electroanal Chem 300:543. doi:10.1016/0022-0728(91)85415-L
9. Colletti LP, Teklay D, Stickney JL (1994) J Electroanal Chem 369:145. doi:10.1016/0022-0728(94)87092-6
10. Stickney JL (2001) In: Alkire RC, Kolb DM (eds) Advances in Electrochemistry and Electrochemical Engineering, vol. 7. Wiley, New York, p 1
11. Guidelli R, Innocenti M, Aloisi G, Cavallini M, Pezzatini G, Foresti LM (1998) J Phys Chem B 102:7413. doi:10.1021/jp9811777
12. Demir U, Shannon C (1996) Langmuir 12:6091. doi:10.1021/la960225g
13. Yang JY, Zhu W, Gao XH, Bao SQ, Fan XA (2005) J Electroanal Chem 577:117. doi:10.1016/j.jelechem.2004.11.023
14. Zhu W, Yang JY, Gao XH, Bao SQ, Fan XA, Zhang TJ, Cui K (2005) Electrochim Acta 50:4041. doi:10.1016/j.electacta.2005.01.003
15. Qiao ZH, Shang W, Wang CM (2005) J Electroanal Chem 576:171. doi:10.1016/j.jelechem.2004.10.015
16. Huang BM, Coletti LP, Gregory BW, Anderson JL, Stickney JL (1995) J Electrochem Soc 142:3007. doi:10.1149/1.2048677
17. Coletti LP, Flowers BH, Stickney JL (1998) J Electrochem Soc 145:1442. doi:10.1149/1.1838502
18. Maestre MS, Rodrigez-Amaro R, Munoz E, Ruiz JJ, Camacho L (1994) J Electroanal Chem 373:31. doi:10.1016/0022-0728(94)03317-X
19. Bewick A, Fleischmann M, Thirsk HR (1962) Trans Faraday Soc 58:2200. doi:10.1039/tf9625802200
20. Fleischmann M, Thirsk HR (1963) In: Delahay P (ed) Advances in electrochemistry and electrochemical engineering, vol 3. Wiley, New York, p 00
21. Huang BM, Lister TE, Stickney JL (1997) Surf Sci 392:27. doi:10.1016/S0039-6028(97)00413-5
22. Alanyalioglu M, Demir U, Shannon C (2004) J Electroanal Chem 561:21. doi:10.1016/j.jelechem.2003.07.016
23. Greenwood NN, Earnshaw A (1984) Chemistry of the elements. Pergamon, Oxford, p 756
24. Wei C, Myung N, Rajeshwar K (1994) J Electroanal Chem 375:109. doi:10.1016/0022-0728(94)03377-3
25. Solaliendres MO, Manzoli A, Salazar-Banda GR, Eguiluz KIB, Tanimoto ST, Machado SAS (2008) J Solid State Electrochem 12:679. doi:10.1007/s10008-007-0401-6
26. Bosco E, Rangarajan SK (1981) J Electroanal Chem 129:25. doi:10.1016/S0022-0728(81)80003-4
27. Bhattacharjee B, Rangarajan SK (1991) J Electroanal Chem 302:207. doi:10.1016/0022-0728(91)85041-M
28. Manuel PP, Margarita MH, Ignacio G, Nikola B (1998) Surf Sci 399:80. doi:10.1016/S0039-6028(97)00813-3
29. Manuel PP, Ignacio G, Nikola B (2000) J Phys Chem B 104:3545. doi:10.1021/jp9931861
30. Budevski EB (1983) In: Conway BE, Bockris JO'M, Yeager E, Kahn SUM, White RE (eds) Comprehensive treatise of electrochemistry, vol 7. Plenum, New York, p 399